Physics Letters B 782 (2018) 633–640

Contents lists available at ScienceDirect

Physics Letters B

www.elsevier.com/locate/physletb

Status of neutrino oscillations 2018: 3σ hint for normal mass ordering and improved CP sensitivity ☆

P.F. de Salas [a], D.V. Forero [b,c], C.A. Ternes [a], M. Tórtola [a,*], J.W.F. Valle [a]

[a] AHEP Group, Institut de Física Corpuscular – CSIC/Universitat de València, Parc Cientific de Paterna, C/ Catedratico José Beltrán, 2 E-46980 Paterna (València), Spain
[b] Instituto de Física Gleb Wataghin – UNICAMP, 13083-859, Campinas, SP, Brazil
[c] Center for Neutrino Physics, Virginia Tech, Blacksburg, VA 24061, USA

ARTICLE INFO

Article history:
Received 4 August 2017
Received in revised form 8 June 2018
Accepted 9 June 2018
Available online 14 June 2018
Editor: A. Ringwald

Keywords:
Neutrino mass and mixing
Neutrino oscillation
Solar and atmospheric neutrinos
Reactor and accelerator neutrinos
Neutrino telescopes

ABSTRACT

We present a new global fit of neutrino oscillation parameters within the simplest three-neutrino picture, including new data which appeared since our previous analysis [1]. In this update we include new long-baseline neutrino data involving the antineutrino channel in T2K, as well as new data in the neutrino channel, data from NOνA, as well as new reactor data, such as the Daya Bay 1230 days electron antineutrino disappearance spectrum data and the 1500 live days prompt spectrum from RENO, as well as new Double Chooz data. We also include atmospheric neutrino data from the IceCube DeepCore and ANTARES neutrino telescopes and from Super-Kamiokande. Finally, we also update our solar oscillation analysis by including the 2055-day day/night spectrum from the fourth phase of the Super-Kamiokande experiment. With the new data we find a preference for the atmospheric angle in the upper octant for both neutrino mass orderings, with maximal mixing allowed at $\Delta\chi^2 = 1.6\,(3.2)$ for normal (inverted) ordering. We also obtain a strong preference for values of the CP phase δ in the range $[\pi, 2\pi]$, excluding values close to $\pi/2$ at more than 4σ. More remarkably, our global analysis shows a hint in favor of the normal mass ordering over the inverted one at more than 3σ. We discuss in detail the status of the mass ordering, CP violation and octant sensitivities, analyzing the interplay among the different neutrino data samples.

1. Introduction

The discovery of neutrino oscillations constitutes a major milestone in astro and particle physics over the last few decades. Solar and atmospheric neutrino studies were the first to give a convincing evidence for neutrino conversion [2,3]. By studying the distortion in the neutrino spectra, laboratory experiments based at reactors and accelerators have played a key role in selecting neutrino oscillations as the conversion mechanism at work. Reactor and accelerator experiments have now brought the field of neutrino oscillations to the precision era, contributing significantly to sharpen the determination of the oscillation parameters [4–9]. Particularly relevant was the input of the KamLAND experiment in elucidating the nature of the solution to the solar neutrino puzzle [10,11]. Indeed, KamLAND measurements have ruled out alternative mechanisms involving spin flavor precession [12,13] as well as nonstandard neutrino interaction (NSI) solutions to the solar neutrino problem [14]. Such NSI-only scenarios as well as all other more exotic hypotheses are all ruled out by KamLAND [15,5].

Precision tests of the oscillation picture have already a long history, and remain as timely as ever. Indeed, one can probe neutrino NSI with atmospheric [16] as well as solar neutrino data [17,18], where the robustness of the solar neutrino oscillation description has been questioned [19,20]. There have been a variety of studies scrutinizing the possible role of NSI in various neutrino oscillation setups [21–35]. Likewise, although already constrained by experiment, the effect of neutrino non-unitarity of the lepton mixing matrix, expected if neutrino masses arise *a la seesaw* [36–38], could lead to important ambiguities in probing CP violation in neutrino oscillations [39], as well as opportunities for probing novel effects. These need to be taken up seriously in the design of future oscillation experiments [40–42]. One example are neutrino factories,

☆ https://globalfit.astroparticles.es/.

* Corresponding author.
E-mail addresses: pabferde@ific.uv.es (P.F. de Salas), dvanegas@ifi.unicamp.br (D.V. Forero), chternes@ific.uv.es (C.A. Ternes), mariam@ific.uv.es (M. Tórtola), valle@ific.uv.es (J.W.F. Valle).

https://doi.org/10.1016/j.physletb.2018.06.019

which also provide a potential testing ground for the non-unitarity of the neutrino mixing matrix [43,44].

Similarly, neutrino magnetic moment interactions in turbulent convective-zone magnetic fields would induce an enhanced solar antineutrino flux, to which KamLAND observations are sensitive [12,13]. Likewise, radiative-zone random magnetic fields [45] would induce sizeable density fluctuations, capable of affecting neutrino propagation in a significant manner [46,47]. However, under the hypothesis of CPT conservation, KamLAND constrains the effect of potentially large density fluctuations on solar neutrino oscillations [48,49].

Here we reconsider the determination of neutrino oscillation parameters within the simplest three-neutrino picture, in the light of new data that appeared since our previous published global analysis [1]. These include new long-baseline disappearance and appearance data involving the antineutrino channel in T2K [50,51], an updated dataset in the neutrino mode [52], as well as disappearance and appearance neutrino data from NOνA [53–55]. Turning to reactors, we have included the electron antineutrino disappearance spectrum of Daya Bay corresponding to 1230 days of data [56], the 1500 live days prompt reactor spectra from RENO [57,58] as well as the Double Chooz event energy spectrum from the far-I and far-II data periods [59]. Concerning atmospheric neutrinos, we have included data from the IceCube DeepCore [60] and ANTARES [61] neutrino telescopes, properly taking into account the relevant matter effects in the neutrino propagation inside the Earth. Given the difficulties to analyze the most recent atmospheric neutrino data from Super-Kamiokande with the public information available, we directly include the χ^2-tables provided by the Super-Kamiokande Collaboration, corresponding to the combination of the four run periods of the experiment [62]. Finally, we have also updated our solar oscillation analysis by including the 2055-day day/night spectrum from the fourth phase of the Super-Kamiokande experiment [63].

2. New experiments

In this section we present a brief description of the NOνA long-baseline accelerator neutrino experiment as well as the neutrino telescopes ANTARES and IceCube DeepCore which were not included in the previous global fit [1].

2.1. The ANTARES neutrino telescope

ANTARES is a deep sea neutrino telescope located at the Mediterranean Sea, near Toulon (France). It consists of 12 lines with 75 optical modules each, covering a height of 350 m and anchored at the sea floor at a depth of about 2.5 km, with a separation of around 70 m between neighboring modules. The neutrino detection is based on the Cherenkov light emitted when the charged leptons produced by the neutrino interactions move through the water. Although ANTARES was not designed to contribute to the determination of the oscillation parameters, it was the first large volume Cherenkov-based neutrino telescope performing such analysis with atmospheric neutrinos. They managed to do it as a result of an important reduction of their threshold energy, from 50 GeV, when only multi-line events are considered, to 20 GeV for single-line events.

2.2. IceCube DeepCore

IceCube is a 1 km^3 multipurpose neutrino telescope placed near the Amundsen–Scott South Pole Station, buried beneath the surface and extending up to a depth of about 2500 meters. Similarly to ANTARES, it uses Cherenkov light to detect high energy neutrinos, with the difference that IceCube uses the polar ice as the medium where this light is produced. It has 86 strings with 60 digital optical modules (DOMs) each, placed at a depth that goes from 1450 m to 2450 m into the ice. In this analysis we use the data from DeepCore, a denser region of strings inside IceCube, designed to measure the atmospheric neutrino flux at low energies. The observed energy lies between 6.3 GeV and 56.2 GeV, way below the energy threshold of IceCube, which is about 100 GeV.

2.3. The NOνA experiment

The NOνA experiment is a long-baseline neutrino oscillation facility, with a 810 km baseline, which makes it the biggest long baseline experiment to date. It was designed to observe ν_μ-disappearance as well as ν_e-appearance in both neutrino and antineutrino channels. In order to accomplish this, it uses an intense and (nearly) pure beam of ν_μ generated at the Fermilab accelerator complex. These neutrinos go through the Earth to northern Minnesota, 810 km away, to be detected at the Ash River far detector. The NOνA experiment has collected an equivalent of 8.85×10^{20} protons on target of data in the neutrino mode and is now taking data with the antineutrino beam. Because of its 810 km baseline, it is more sensitive to matter effects than the T2K experiment. With further data taking, this may translate into a better sensitivity to the neutrino mass ordering. The detectors are 14 mrad off-axis, which results in a narrow neutrino energy spectrum, peaked around 2 GeV, which coincides with the oscillation maximum for $\nu_\mu \to \nu_e$ oscillations.

3. New data

We now describe the new data samples used in this updated global neutrino oscillation analysis.

3.1. Updated solar neutrino data sample

We have updated our solar oscillation analysis including the 2055-day D/N (day/night) spectrum from the fourth phase of the Super-Kamiokande experiment, according to Ref. [63]. This new sample includes the D/N energy spectrum above 3.5 MeV collected along 2055 days, from September 2008 to April 2015. The signal observed corresponds to a ^{8}B solar neutrino flux of $2.314 \pm 0.018(\text{stat}) \pm 0.039(\text{syst}) \times 10^6$ cm^{-2}s^{-1}. The measured D/N asymmetry during this period is determined as $A_{DN} = [-3.1 \pm 1.6(\text{stat}) \pm 1.4(\text{syst})]$ %, at 1.5σ from zero. Thanks to the increasing accuracy, this result combined with the observed D/N asymmetry in the three previous phases of Super-K, provides an indirect indication for matter-enhanced neutrino oscillations inside the Earth. Apart from small differences in the values of the oscillation parameters, the main results concerning the neutrino oscillation parameters remain intact with respect to our previous analysis in [1], in particular the fact that maximal solar neutrino mixing is highly disfavored.[1]

3.2. New data from Daya Bay

Daya Bay is a multi-core and multi-detector experiment, with eight 20 ton Gd-doped liquid scintillator antineutrino detectors (ADs) located at three experimental halls (EHs). At EH1 and EH2,

[1] The reanalysis of KamLAND data in the light of the recently observed "bump" in the reactor antineutrino spectrum might produce small deviations of the solar oscillation parameters, as obtained in Ref. [64].

two ADs were deployed while the remaining ADs were assigned to the far site, EH3. The thermal power of each reactor is 2.9 GW_{th} and the baseline to the near and far sites (EH1 and EH2) are in the range 0.35–0.6 km and 1.5–1.9 km, respectively. After 1230 days of data taking, Daya Bay has measured approximately two hundred thousand inverse beta decay events at the far site. Thanks to the large statistics and the reduction of systematical errors, due to having several functionally identical ADs, Daya Bay has provided the most precise determination of the reactor mixing angle to date.

In this analysis, we have included the antineutrino event energy spectra from the three EHs. Systematical errors accounting for total and detector normalization, as well as core-related errors and energy scale errors were included in the analysis. Systematical errors accounting for the background normalization in each experimental hall have been also included in the analysis, where we have used the background expectations from the ancillary files from Ref. [56].

3.3. New data from RENO

The RENO experiment has recently reported 1500 live days of data from antineutrinos produced at six reactor cores each one with a ~ 2.8 GW_{th} thermal power. The experiment detects neutrinos at a near and at a far detector (each detector with 16 ton of fiducial mass) located at 0.294 km and 1.383 km from the line joining the six reactor cores, respectively.[2] Thanks to the improved precision, the spectral fit analysis of RENO data is now sensitive to the neutrino oscillation phase, as reported in Refs. [57,58]. In our analysis, we have considered the near and far detector event energy distribution. We have fitted the measured energy spectrum at each detector after the subtraction of the background, normalizing our simulation to the expected spectra reported by the RENO Collaboration. Systematical errors accounting for core-related (0.9% for each core) and detector uncertainties (0.2% for each detector) [66], have been included in our analysis in the form of nuisance parameters. We have also included a nuisance parameter accounting for the total normalization uncertainty, that has been left completely free in the analysis.

3.4. New data from Double Chooz

The Double Chooz experiment detects antineutrinos produced at two reactor cores with a 2×4.27 GW_{th} total thermal power with a near and far detector of 8 ton fiducial mass each, located at 0.4 km and 1.05 km, respectively. The data set considered in this analysis corresponds to 461 days of data with far detector only (far-I) plus 212 days of far detector data with a near detector (far-II), as reported in Ref. [59].[3] The event energy spectrum from the far-I and far-II data periods were included in the analysis. Systematical errors considered in our simulation account for the signal and background normalization as well as for the total normalization. The total background has been extracted from the data reported in Ref. [59]. The results of the analysis of the three reactor experiments are given in Fig. 1 and will be discussed in detail in the next section.

3.5. Atmospheric data from ANTARES

We analyze atmospheric data from the ANTARES Collaboration following Ref. [61], taking also into account matter effects, and including electron neutrino and neutral current interaction events. In order to calibrate our simulation we have first reproduced very well the analysis performed by the collaboration using their assumptions and approximations. Afterwards we have included neutral current interactions and matter effects to our simulation. In Fig. 2 we plot the allowed regions in the atmospheric parameters at 90 and 99% C.L. from our analysis of ANTARES data. One sees the regions are still very large and therefore the sensitivity is not competitive with the other experiments, described in the following sections. It is expected that the ANTARES Collaboration will update their analysis with more data, hopefully improving their sensitivity to the atmospheric neutrino oscillation parameters.

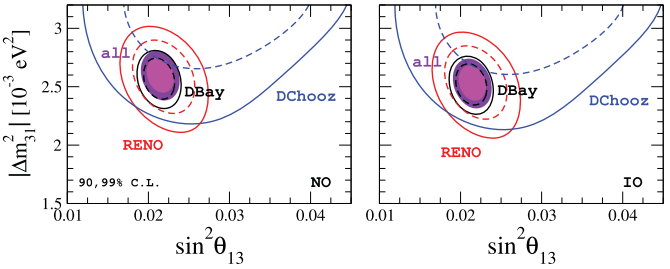

Fig. 1. 90 and 99% C.L. (2 d.o.f.) allowed regions at the $\sin^2\theta_{13}$–Δm^2_{31} plane from individual reactor neutrino experiments (dashed and solid lines) and from the combination of the three experiments (colored regions). The left (right) panels correspond to normal (inverted) mass ordering.

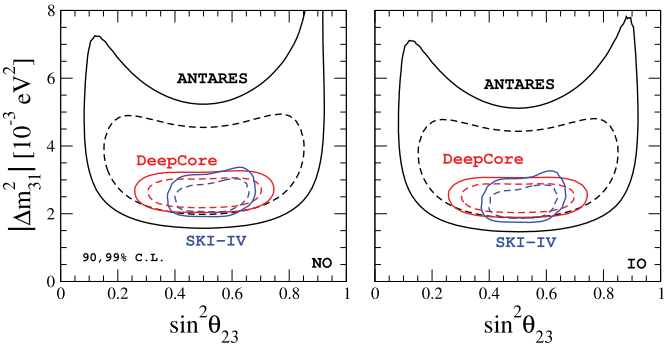

Fig. 2. 90 and 99% C.L. (2 d.o.f.) allowed regions at the $\sin^2\theta_{23}$–Δm^2_{31} plane obtained from the atmospheric neutrino experiments for normal (left) and inverted ordering (right).

3.6. Atmospheric data from IceCube DeepCore

In order to determine the atmospheric neutrino oscillation parameters, in this simulation we use data published by IceCube DeepCore in Ref. [60], analyzed following all the updates presented by the collaboration. Neutrino data are presented in 64 bins, with 8 energy-bins and 8 bins in zenith-angle, see [68]. Tables with systematic detector uncertainties, optical efficiencies and uncertainties produced through scattering at holes opened in the ice for the depletion of the DOMs are also provided. The fluxes for atmospheric neutrinos are taken from [69,70]. We perform the numerical integration in matter using the Preliminary Reference Earth Model (PREM) [71]. In Fig. 2 we compare the allowed regions in the atmospheric neutrino oscillation parameters $\sin^2\theta_{23}$ and Δm^2_{31} obtained from ANTARES, DeepCore and Super-Kamiokande phases I–IV at 90 and 99% confidence level. As discussed in the next section, with such new analysis, DeepCore data are becoming compet-

[2] The exact detector to reactor distances from Ref. [65] were used in our simulation.

[3] Even though more recent data has been presented at the Moriond conference [67], the collaboration is still trying to understand better their systematics. For this reason we have only included the previous data from [59] in our analysis.

itive with those of long-baseline experiments NOνA or T2K in the determination of the atmospheric neutrino oscillation parameters.[4]

3.7. Atmospheric data from Super-Kamiokande

In this work we include the most recent atmospheric neutrino results from the Super-Kamiokande experiment [62], corresponding to the combined analysis of phases I to IV of the experiment, with a total of 328 kton-year exposure of the detector. The data analysis performed by the Super-K Collaboration, optimized to enhance the sensitivity to the neutrino mass ordering, includes the impact of the atmospheric oscillation parameters as well as the reactor angle and the CP phase. As stressed in [73], the most recent atmospheric neutrino Super-K data samples are not presented in a form that allows a reliable use outside the collaboration. Therefore, here we follow the same procedure adopted in previous publications (Refs. [1,74,75]) which consists of directly incorporating to our global neutrino analysis the χ^2-tables provided by the Super-K Collaboration [76], obtained in Ref. [62].

3.8. New long-baseline data from T2K

In addition to the data used in the neutrino oscillation global fit published in Ref. [1], the T2K Collaboration has new results in the neutrino mode. Therefore, this updated analysis includes the latest T2K antineutrino sample as well as their updated neutrino data, as published in Refs. [50–52]. With an accumulated statistics of 14.6×10^{20} POT in the neutrino run, the T2K Collaboration now observes 240 disappearance and 74+15 appearance (charged current quasi-elastic and charged current single-pion, respectively) neutrino events. Note, however, that the CC-1π appearance events have not been included in our simulation. In the antineutrino channel, with 7.6×10^{20} POT, a total of 68 disappearance $\bar{\nu}_\mu$ events and 7 appearance $\bar{\nu}_e$ events were recorded. In the present analysis we have included the newest neutrino fluxes in Super-K provided by the T2K web page [77]. The simulation of the experiment and the statistical analysis were performed with the GLoBES package [78,79], including all systematic uncertainties reported in Ref. [52].

Notice that T2K has already achieved some CP sensitivity, as seen in Fig. 4. Indeed, thanks to the combination of the results in the neutrino and the antineutrino channel, T2K is the first experiment able to exclude on its own certain values of the CP phase at more than 2σ for normal ordering (NO), and even at 3σ for inverted ordering (IO). The allowed regions for other oscillation parameters, such as θ_{13} and Δm^2_{31}, are found to be consistent with the reactor experiments.

3.9. New long-baseline data from NOνA

In our global fit we also include the latest results for ν_μ-disappearance and ν_e-appearance of the NOνA experiment. NOνA has recently published the results of their neutrino run with an accumulated statistics of 8.85×10^{20} POT [55]. In the disappearance channel, a total of 126 events have been observed, while 763 events were expected under the no-oscillation hypothesis. In the appearance channel, a total of 66 events have been detected. The neutrino oscillation analysis reported by the NOνA Collaboration imposing a prior on θ_{13} slightly disfavors inverted mass ordering, with a significance of approximately 2σ. Our simulation of the NOνA experiment has been performed using GLoBES [78,79], including all the systematic errors reported in [53,54] and updated in Ref. [55].

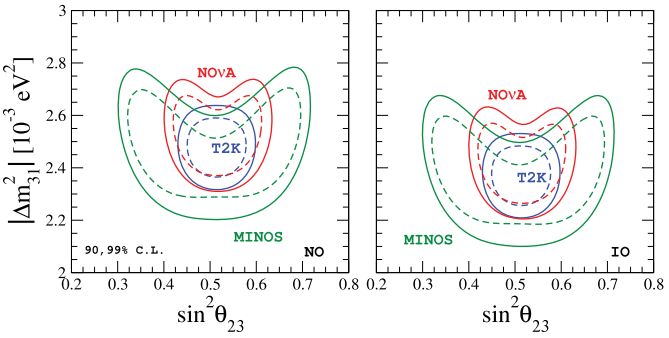

Fig. 3. 90 and 99% C.L. (2 d.o.f.) allowed regions at the $\sin^2\theta_{23}$–Δm^2_{31} plane for normal (left) and inverted mass ordering (right) as restricted from the long-baseline experiments.

In Fig. 3 we compare the restrictions on the atmospheric neutrino parameters derived from long-baseline accelerator data coming from the T2K, NOνA and MINOS experiments, at 90 and 99% confidence level. Further results are summarized in Figs. 4, 5, 6, 7 and 8 and discussed in the following section.

4. Global fit results

We now describe the global results of our updated neutrino oscillation fit. There are no significant changes derived from the new solar neutrino data, hence we move directly to the results for atmospheric neutrinos. Here there are new data from the ANTARES and IceCube Collaborations as well as from Super-Kamiokande phase IV. As seen in Fig. 2, the 863-day atmospheric data from ANTARES and the 3-year data from IceCube DeepCore are enough to provide a determination of the atmospheric oscillation parameters. Note, however, that the determination of θ_{23} from atmospheric data is still dominated by the analysis of Super-Kamiokande. In any case, the neutrino telescope results are in complete consistency with what follows from the Super-Kamiokande atmospheric data, leading to a clear global picture for the all-atmospheric data fit, shown in Fig. 2.

Concerning the long-baseline accelerator data, Fig. 3 shows the allowed regions by the latest NOνA and T2K neutrino results, as well as the older MINOS data sample. In comparison with Fig. 2, one sees that atmospheric parameters are mainly constrained by long-baseline data, and that now all the results are in agreement with maximal atmospheric mixing. On the other hand, Fig. 1 shows how the new reactor data, clearly dominated by Daya Bay, provide a significantly improved determination of θ_{13}. It also illustrates the important role of reactor neutrino data in mapping out the allowed region of the atmospheric squared mass splitting parameter.

In what follows we highlight the main features of our neutrino oscillation global fit results, focusing upon the main open challenges of the three-neutrino picture: CP violation, the neutrino mass ordering and the θ_{23} octant problem.

4.1. Sensitivity to CP violation

Long-baseline neutrino oscillation data play an important role in determining the CP violating phase, δ. In order to highlight this point we present the $\Delta\chi^2$-profile for the CP phase, as determined from T2K, NOνA and Super-K atmospheric data alone, as well as by the global oscillation data sample, as shown in the right panels in Fig. 4. Note that here the $\Delta\chi^2$-profile has been obtained from the local minimum for each mass ordering.

[4] The recent reanalysis of DeepCore data performed by the IceCube Collaboration in Ref. [72] shows improved sensitivity to the atmospheric neutrino oscillation parameters. However, the details of this reanalysis are not yet publicly available, so this improvement cannot be incorporated in our global fit.

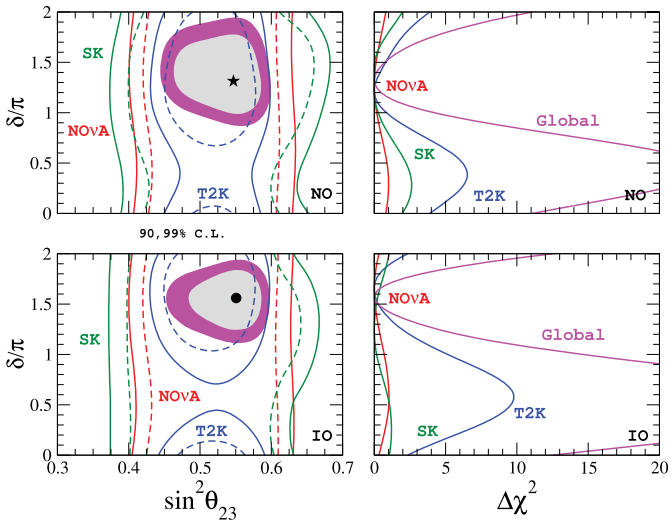

Fig. 4. Left: 90 and 99% C.L. (2 d.o.f.) regions from T2K (blue lines) and NOνA (red) data, from the atmospheric Super-K results (green) and from the global fit of all the oscillation experiments (colored regions). The star indicates the best fit point from our global analysis, found for normal mass ordering, while the black dot indicates the local minimum for inverted mass ordering. Right: $\Delta\chi^2$-profile as a function of the CP phase δ from T2K, NOνA and Super-K atmospheric (with the same color code as in the left panel) and from the global fit (magenta). In both cases, the upper (lower) panels correspond to normal (inverted) mass ordering. (For interpretation of the colors in the figure(s), the reader is referred to the web version of this article.)

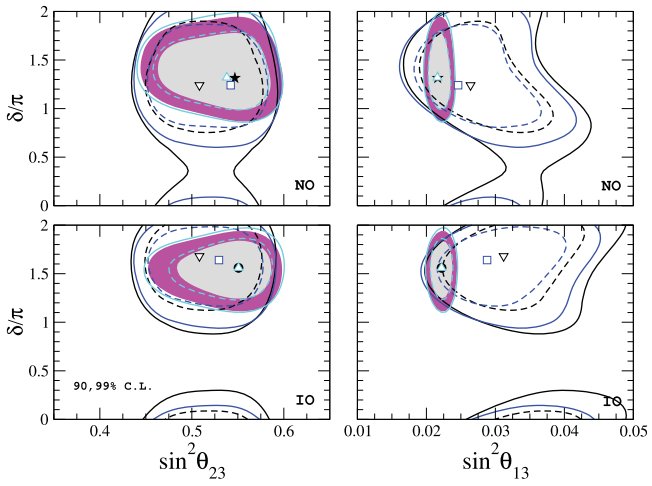

Fig. 5. 90 and 99% C.L. (2 d.o.f.) allowed regions in the $\sin^2\theta_{23}$–δ (left) and $\sin^2\theta_{13}$–δ (right) planes from long-baseline data only (black lines), long-baseline plus atmospheric (blue), long-baseline plus reactors (cyan) and from the global fit of all experiments (colored regions). Upper (lower) panels correspond to normal (inverted) mass ordering. The best fit points are indicated by black down-triangles (long-baseline data), blue squares (long-baseline plus atmospheric), cyan up-triangles (long-baseline plus reactors), as well as stars and black dots, following the same convention as in Fig. 4.

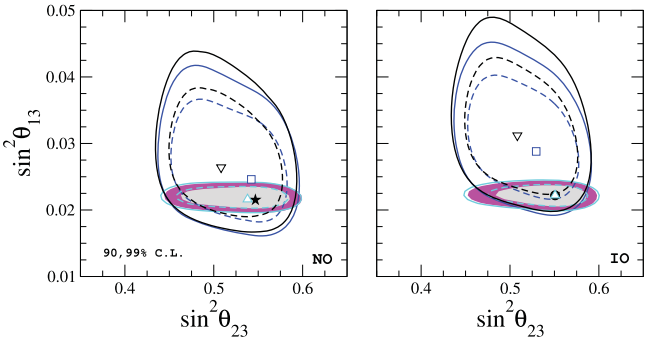

Fig. 6. 90 and 99% C.L. (2 d.o.f.) regions from the combination of different neutrino data samples. The convention used to indicate the regions and best fit points is the same as in Fig. 5.

This result shows how the current global sensitivity to the CP phase is dominated by the T2K experiment, with added rejection against $\delta = \pi/2$ obtained after combining with the other experiments. Indeed, we find that the combination with reactor data is crucial to enhance the rejection against $\delta = \pi/2$. As a result, we find that in the global analysis, $\delta = \pi/2$ is disfavored with $\Delta\chi^2 = 22.9$ (4.8σ) for normal ordering. The rejection against $\delta = \pi/2$ is found to be stronger for inverted mass spectrum, where it is excluded with $\Delta\chi^2 = 37.3$ (6.1σ), with respect to the minimum for this ordering. As can also be seen from the figure, the current preferred value of δ depends on the mass ordering, lying closer to $3\pi/2$ for inverted ordering. The current best fit values for the CP violating phase are located at $\delta = 1.32\pi$ for NO and at $\delta = 1.56\pi$ for IO.

4.2. Neutrino mass ordering

Concerning the sensitivity to the neutrino mass ordering, our global fit shows for the first time a hint in favor of normal neutrino mass ordering, with inverted ordering disfavored with $\Delta\chi^2 = 11.7$ (3.4σ). In order to disentangle the origin of the preference for NO in our global analysis, we display in Figs. 5 and 6 the allowed regions for θ_{23}, θ_{13} and δ for NO and IO for different data set combinations: long-baseline data only, long-baseline plus atmospheric, long-baseline plus reactors and the combination of all data sets. Down-triangles indicate the best fit points obtained in the analysis of long-baseline data, squares correspond to the best fit points derived from the combination of long-baseline plus atmospheric, while up-triangles are the best fit point for long-baseline plus reactor data. The star and black dot follow the same convention as in Fig. 4.

The black lines in these figures delimit the allowed regions from the combination of all long-baseline data discussed above. In principle, given the small impact of matter effects in the neutrino propagation at such baselines, one would expect a limited sensitivity of the current long-baseline experiments to the neutrino mass ordering. Indeed, this is confirmed by our independent analysis of T2K and NOνA data, that show only a slight preference for normal mass ordering at the level of $\Delta\chi^2 \sim 1$. However, the combined analysis of long-baseline and reactor data (see cyan lines in the figures) results in an enhanced sensitivity to the mass ordering which, in all cases, favors normal over inverted mass ordering. This happens due to the mismatch between the values of θ_{13} preferred by reactor and long-baseline experiments, which is larger for the inverted mass ordering, as shown in Figs. 5 and 6. While in normal ordering the best fit for long-baseline experiments alone, $\sin^2\theta_{13} = 0.026$, is relatively close to the global one, $\sin^2\theta_{13} \simeq 0.022$, mainly constrained by reactors, this is not the case for inverted ordering, where long-baseline data prefer $\sin^2\theta_{13} = 0.031$. As a result, the combined analysis of reactor and long-baseline data shows better agreement under the normal mass ordering hypothesis. For instance, a combined analysis of the latest NOνA results with reactor data indicates a preference for normal ordering with $\Delta\chi^2 = 3.7$. In the case of T2K, the combination with reactor data results in a stronger preference for normal over inverted mass ordering, with $\Delta\chi^2 = 5.3$. This enhanced sensitivity to the mass ordering is due to the tension that exists between the value of the atmospheric mass splitting preferred by reactor, mainly Daya Bay, and T2K. One finds that Daya Bay prefers a higher value for Δm^2_{31} with respect to the one indicated by T2K, and the difference

is larger for inverted mass ordering. The combined analysis of all long-baseline and reactor data yields a preference for normal mass ordering with $\Delta\chi^2 = 7.5$.

By combining these data samples with atmospheric data, one gets the final global results indicated by the colored regions in Figs. 5 and 6. In principle, one may expect the largest sensitivity to the neutrino mass ordering to come from the observation of matter effects in the atmospheric neutrino flux. However, we find that the neutrino telescope experiments IceCube DeepCore and ANTARES are not yet very sensitive to the mass ordering. In fact, the difference between normal and inverted mass ordering from the combined analysis of DeepCore and ANTARES is only $\Delta\chi^2 = 0.4$, obtained mainly from IceCube DeepCore data. On the other hand, the most recent analysis of atmospheric data sample of the Super-K experiment shows an enhanced sensitivity to the mass ordering compared to previous ones. Indeed, Super-K data alone disfavors the inverted mass ordering with $\Delta\chi^2 = 3.5$. If a prior on the reactor mixing angle is imposed in the atmospheric data analysis, the sensitivity rises up to $\Delta\chi^2 = 4.3$ [62]. The effect of adding the atmospheric data to the global analysis is not very noticeable in Figs. 5 and 6, where the allowed regions with and without atmospheric data are similar. However, the impact of atmospheric data in the global sensitivity to the mass ordering allows one to disfavor inverted mass ordering at $\Delta\chi^2 = 11.7$. This result is very relevant, since from the combination of the different types of neutrino experiments we can obtain for the first time a preference for normal neutrino mass ordering slightly above 3σ.

4.3. The θ_{23} octant problem

The role of long-baseline, atmospheric and reactor experiments in selecting the θ_{23}-octant is illustrated in Figs. 5 and 6. They stress the complementary role of the different oscillation data samples on the possible discrimination of the θ_{23} octant. In fact, as noticed in Ref. [80] and recently in Ref. [81], an improved measurement of the reactor angle helps resolving the atmospheric octant. From the figures, we see that the analysis of long-baseline data only (indicated by black lines) shows a preference for values of θ_{23} close to maximal mixing for the two mass orderings, with the best fit points indicated by a down-triangle. For both mass orderings we find a preferred value of $\sin^2\theta_{23} = 0.508$. The combination with the atmospheric data sets (illustrated by the blue lines in the figures) provides a further constraint on the allowed region for θ_{23}. Moreover, the inclusion of atmospheric data in the analysis produces a shift of the best fit value of θ_{23} to larger values for both mass orderings ($\sin^2\theta_{23} = 0.54$ for NO and $\sin^2\theta_{23} = 0.53$ for IO), although values of θ_{23} in the first octant are still allowed with $\Delta\chi^2 \geq 0.8\,(2.0)$ for NO (IO). The combination with reactor experiments in the global neutrino fit (colored regions in the figures) moves the best fit value of θ_{23} to larger values for both mass orderings, leading to $\sin^2\theta_{23} \simeq 0.55$ as the preferred value. Moreover, reactor data also modify the preferred values of θ_{13} and δ, from the values fixed by the combination of long-baseline and atmospheric data, as shown in Figs. 5 and 6. For both mass orderings δ is pushed towards $3\pi/2$, while the reactor mixing angle is slightly shifted towards smaller values. One should stress that reactor data, specially Daya Bay and RENO, are crucial to the determination of the allowed region for θ_{13}. Going back to the octant preference, we would like to remark that the indications described above are still far from robust. Indeed, values of the atmospheric mixing angle below 45° are allowed at $\Delta\chi^2 \geq 1.6$ for the case of normal ordering and at $\Delta\chi^2 \geq 3.2$ for inverted ordering with respect to the minimum in this mass spectrum.

Despite the recent progress on this matter, the octant discrimination problem lies far beyond the current generation of neutrino oscillation experiments, and will be a particularly stubborn problem in the years to come. On the positive side, however, it has been noted that the task of octant discrimination and probing for leptonic CP violation in current and future long-baseline experiments can be facilitated by prior model-specific theoretical knowledge of the predicted pattern of leptonic mixing. See, as an example, Figure 1 given in [82] and the associated discussion.

Table 1
Neutrino oscillation parameters summary determined from this global analysis. The ranges for inverted ordering refer to the local minimum for this neutrino mass ordering.

Parameter	Best fit $\pm 1\sigma$	2σ range	3σ range
Δm^2_{21} [10^{-5}eV^2]	$7.55^{+0.20}_{-0.16}$	7.20–7.94	7.05–8.14
$\lvert\Delta m^2_{31}\rvert$ [10^{-3}eV^2] (NO)	2.50 ± 0.03	2.44–2.57	2.41–2.60
$\lvert\Delta m^2_{31}\rvert$ [10^{-3}eV^2] (IO)	$2.42^{+0.03}_{-0.04}$	2.34–2.47	2.31-2.51
$\sin^2\theta_{12}/10^{-1}$	$3.20^{+0.20}_{-0.16}$	2.89–3.59	2.73–3.79
$\theta_{12}/^\circ$	$34.5^{+1.2}_{-1.0}$	32.5–36.8	31.5–38.0
$\sin^2\theta_{23}/10^{-1}$ (NO)	$5.47^{+0.20}_{-0.30}$	4.67–5.83	4.45–5.99
$\theta_{23}/^\circ$	$47.7^{+1.2}_{-1.7}$	43.1–49.8	41.8–50.7
$\sin^2\theta_{23}/10^{-1}$ (IO)	$5.51^{+0.18}_{-0.30}$	4.91–5.84	4.53–5.98
$\theta_{23}/^\circ$	$47.9^{+1.0}_{-1.7}$	44.5–48.9	42.3–50.7
$\sin^2\theta_{13}/10^{-2}$ (NO)	$2.160^{+0.083}_{-0.069}$	2.03–2.34	1.96–2.41
$\theta_{13}/^\circ$	$8.45^{+0.16}_{-0.14}$	8.2–8.8	8.0–8.9
$\sin^2\theta_{13}/10^{-2}$ (IO)	$2.220^{+0.074}_{-0.076}$	2.07–2.36	1.99–2.44
$\theta_{13}/^\circ$	$8.53^{+0.14}_{-0.15}$	8.3–8.8	8.1–9.0
δ/π (NO)	$1.32^{+0.21}_{-0.15}$	1.01–1.75	0.87–1.94
$\delta/^\circ$	238^{+38}_{-27}	182–315	157–349
δ/π (IO)	$1.56^{+0.13}_{-0.15}$	1.27–1.82	1.12–1.94
$\delta/^\circ$	281^{+23}_{-27}	229–328	202–349

5. Summary and discussion

We have discussed in detail the status of the mass ordering, CP violation and octant discrimination, analyzing the interplay among the different neutrino oscillation data samples. The results obtained in our global fit are summarized in Table 1 as well as Figs. 7 and 8 for normal and inverted mass ordering. Some comments are in order.

First we note that the improved precision on θ_{13} follows mainly from the Daya Bay and RENO data. Thanks to the combination of T2K neutrino and antineutrino data, we have now an improved sensitivity to CP violation. Indeed, T2K is the first experiment showing a sensitivity on its own, excluding some values of δ before combining with reactor data. In this analysis, we have obtained a strong preference for values of the CP phase in the range $[\pi, 2\pi]$, excluding values close to $\pi/2$ at more than 4σ. Concerning the octant of θ_{23}, this global analysis prefers the second octant slightly, in agreement with the previous one in Ref. [1]. We have found that for normal neutrino mass ordering the upper atmospheric octant is now preferred with $\Delta\chi^2 = 1.6$, while for the case of inverted ordering, values of the atmospheric mixing angle in the lower octant are allowed with $\Delta\chi^2 \geq 3.2$. More remarkably, our global analysis favors for the first time the normal mass ordering over the inverted one at 3.4σ. As discussed in the previous section, part of the sensitivity to the mass ordering comes from the most recent atmospheric analysis of Super-K. This new analysis shows a preference for normal over inverse mass ordering with $\Delta\chi^2 = 3.5$. On the other hand, a mismatch between the values of θ_{13} preferred by long-baseline and reactor data (larger for IO) also gives a relevant contribution to the global sensitivity to the mass ordering.

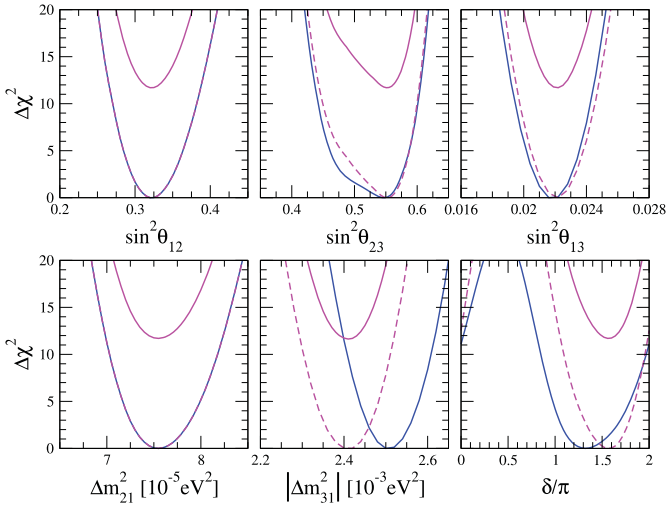

Fig. 7. Summary of neutrino oscillation parameters, 2018. Blue lines correspond to NO and magenta lines to IO. The $\Delta\chi^2$-profiles for inverted ordering are plotted with respect to the minimum for this neutrino mass ordering (dashed) as well as with respect to the global minimum (solid lines).

This effect is also enhanced due to a tension between the preferred values of the atmospheric mass splitting by T2K and reactor experiments.

In short, we have seen how the precision in the determination of the best-known oscillation parameters has improved thanks to the recent long-baseline neutrino oscillation and reactor data. Also the sensitivity to mass ordering, CP violation and the octant of the atmospheric angle has improved, although we are still quite far from a robust measurement, especially of the octant. The presence of new physics beyond the Standard Model may affect significantly the results obtained within the current neutrino oscillation picture. For example, nonstandard neutrino interactions with matter and non-unitary neutrino mixing, expected in seesaw models of neutrino mass generation, may significantly reduce the sensitivities. Conversely, however, such well-motivated beyond-standard scenarios can also bring in new opportunities for current and future long-baseline neutrino oscillation experiments.

Note added

During the peer review of the present work, a new neutrino oscillations global fit appeared in Ref. [83]. Although there are differences in the data samples considered, as well as in the approach followed to incorporate IceCube and short-baseline reactor data, there is a general agreement between the results of the two analyses.

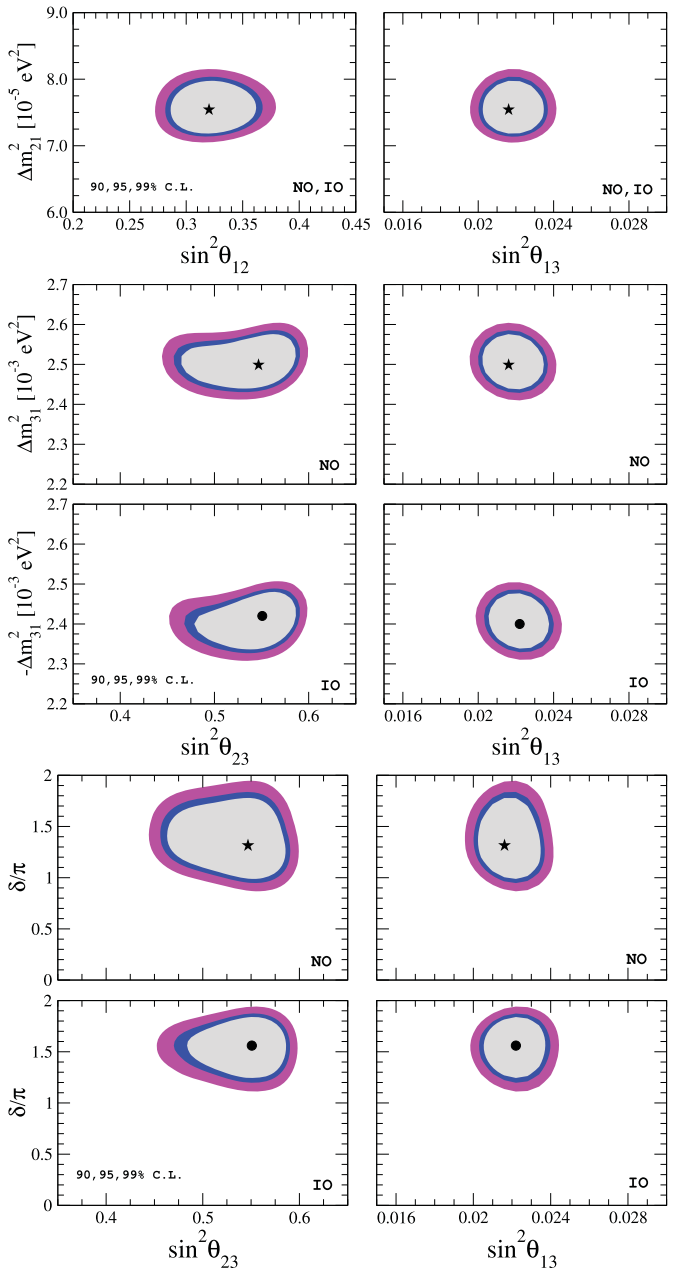

Fig. 8. Global fit summary 2018. In the two four-panel figures, the upper ones correspond to normal ordering and the lower ones to inverted mass ordering. Global fit regions correspond to 90, 95 and 99% C.L. (2 d.o.f.). As in Fig. 7, regions for inverted ordering are plotted with respect to the minimum for this neutrino mass ordering.

Acknowledgements

The authors would like to thank Jason Koskinen of the IceCube Collaboration, Juande Zornoza of the ANTARES Collaboration, Federico Sánchez of T2K and Prof. Soo-Bong Kim of RENO for valuable information regarding their experiments. Likewise, we are grateful to Jordi Salvado and Thomas Schwetz for useful discussions. Work supported by MINECO grants FPA2014-58183-P, FPA2017-85216-P, Multidark-CSD2009-00064, SEV-2014-0398, and the PROMETEOII/2014/084 and GV2016-142 grants from Generalitat Valenciana. MT is also supported a Ramón y Cajal contract RYC-2013-12438 (MINECO). PFdS is supported by the Spanish grant FPU13/03729 (MECD). CAT is supported by the FPI fellowship BES-2015-073593 (MINECO). DVF is thankful for the support of FAPESP Grants No. 2014/19164-6 and 2017/01749-6, and also to FAEPEX Grant No. 2391/17 for partial support. DVF was also supported by the U.S. Department of Energy under contracts DE-SC0013632 and DE-SC0009973.

References

[1] D.V. Forero, M. Tortola, J.W.F. Valle, Phys. Rev. D 90 (2014) 093006, arXiv:1405.7540.
[2] A.B. McDonald, Rev. Mod. Phys. 88 (2016) 030502.
[3] T. Kajita, Rev. Mod. Phys. 88 (2016) 030501.
[4] M. Maltoni, T. Schwetz, J.W.F. Valle, Phys. Rev. D 67 (2003) 093003, arXiv:hep-ph/0212129.
[5] M. Maltoni, T. Schwetz, M.A. Tortola, J.W.F. Valle, New J. Phys. 6 (2004) 122, arXiv:hep-ph/0405172.

[6] H. Nunokawa, S.J. Parke, J.W.F. Valle, Prog. Part. Nucl. Phys. 60 (2008) 338, arXiv:0710.0554.
[7] M.C. Gonzalez-Garcia, M. Maltoni, J. Salvado, T. Schwetz, J. High Energy Phys. 12 (2012) 123, arXiv:1209.3023.
[8] G.L. Fogli, E. Lisi, A. Marrone, D. Montanino, A. Palazzo, A.M. Rotunno, Phys. Rev. D 86 (2012) 013012, arXiv:1205.5254.
[9] A.B. Balantekin, W.C. Haxton, Prog. Part. Nucl. Phys. 71 (2013) 150, arXiv:1303.2272.
[10] K. Eguchi, et al., KamLAND, Phys. Rev. Lett. 90 (2003) 021802, arXiv:hep-ex/0212021.
[11] S. Abe, et al., KamLAND, Phys. Rev. Lett. 100 (2008) 221803, arXiv:0801.4589.
[12] O.G. Miranda, T.I. Rashba, A.I. Rez, J.W.F. Valle, Phys. Rev. Lett. 93 (2004) 051304, arXiv:hep-ph/0311014.
[13] O.G. Miranda, T.I. Rashba, A.I. Rez, J.W.F. Valle, Phys. Rev. D 70 (2004) 113002, arXiv:hep-ph/0406066.
[14] M. Guzzo, P.C. de Holanda, M. Maltoni, H. Nunokawa, M.A. Tortola, J.W.F. Valle, Nucl. Phys. B 629 (2002) 479, arXiv:hep-ph/0112310.
[15] S. Pakvasa, J.W.F. Valle, Proc. Indian Natl. Sci. Acad., A, Phys. Sci. 70 (2004) 189, arXiv:hep-ph/0301061.
[16] N. Fornengo, M. Maltoni, R. Tomas, J.W.F. Valle, Phys. Rev. D 65 (2002) 013010, arXiv:hep-ph/0108043.
[17] A. Bolanos, O.G. Miranda, A. Palazzo, M.A. Tortola, J.W.F. Valle, Phys. Rev. D 79 (2009) 113012, arXiv:0812.4417.
[18] A. Palazzo, J.W.F. Valle, Phys. Rev. D 80 (2009) 091301, arXiv:0909.1535.
[19] O.G. Miranda, M.A. Tortola, J.W.F. Valle, J. High Energy Phys. 10 (2006) 008, arXiv:hep-ph/0406280.
[20] F.J. Escrihuela, O.G. Miranda, M.A. Tortola, J.W.F. Valle, Phys. Rev. D 80 (2009) 105009, arXiv:0907.2630, Phys. Rev. D 80 (2009) 129908 (Erratum).
[21] P. Huber, T. Schwetz, J.W.F. Valle, Phys. Rev. Lett. 88 (2002) 101804, arXiv:hep-ph/0111224.
[22] P. Huber, J.W.F. Valle, Phys. Lett. B 523 (2001) 151, arXiv:hep-ph/0108193.
[23] P. Huber, T. Schwetz, J.W.F. Valle, Phys. Rev. D 66 (2002) 013006, arXiv:hep-ph/0202048.
[24] A. Friedland, C. Lunardini, M. Maltoni, Phys. Rev. D 70 (2004) 111301, arXiv:hep-ph/0408264.
[25] J. Barranco, O.G. Miranda, C.A. Moura, J.W.F. Valle, Phys. Rev. D 73 (2006) 113001, arXiv:hep-ph/0512195.
[26] A. Bandyopadhyay, ISS Physics Working Group, Rep. Prog. Phys. 72 (2009) 106201, arXiv:0710.4947.
[27] A. Esteban-Pretel, J.W.F. Valle, P. Huber, Phys. Lett. B 668 (2008) 197, arXiv:0803.1790.
[28] F.J. Escrihuela, M. Tortola, J.W.F. Valle, O.G. Miranda, Phys. Rev. D 83 (2011) 093002, arXiv:1103.1366.
[29] S.K. Agarwalla, P. Bagchi, D.V. Forero, M. Tortola, J. High Energy Phys. 07 (2015) 060, arXiv:1412.1064.
[30] A. de Gouvea, K.J. Kelly, Nucl. Phys. B 908 (2016) 318, arXiv:1511.05562.
[31] P. Coloma, J. High Energy Phys. 03 (2016) 016, arXiv:1511.06357.
[32] Y. Farzan, J. Heeck, Phys. Rev. D 94 (2016) 053010, arXiv:1607.07616.
[33] D.V. Forero, P. Huber, Phys. Rev. Lett. 117 (2016) 031801, arXiv:1601.03736.
[34] P.F. de Salas, R.A. Lineros, M. Tortola, Phys. Rev. D 94 (2016) 123001, arXiv:1601.05798.
[35] P. Coloma, P.B. Denton, M.C. Gonzalez-Garcia, M. Maltoni, T. Schwetz, J. High Energy Phys. 04 (2017) 116, arXiv:1701.04828.
[36] J.W.F. Valle, Phys. Lett. B 199 (1987) 432.
[37] F.J. Escrihuela, D.V. Forero, O.G. Miranda, M. Tortola, J.W.F. Valle, Phys. Rev. D 92 (2015) 053009, arXiv:1503.08879, Phys. Rev. D 93 (11) (2016) 119905 (Erratum).
[38] O.G. Miranda, J.W.F. Valle, Nucl. Phys. B 908 (2016) 436, arXiv:1602.00864.
[39] O.G. Miranda, M. Tortola, J.W.F. Valle, Phys. Rev. Lett. 117 (2016) 061804, arXiv:1604.05690.
[40] S.-F. Ge, P. Pasquini, M. Tortola, J.W.F. Valle, Phys. Rev. D 95 (2017) 033005, arXiv:1605.01670.
[41] M. Blennow, P. Coloma, E. Fernandez-Martinez, J. Hernandez-Garcia, J. Lopez-Pavon, J. High Energy Phys. 04 (2017) 153, arXiv:1609.08637.
[42] F.J. Escrihuela, D.V. Forero, O.G. Miranda, M. Tortola, J.W.F. Valle, New J. Phys. 19 (2017) 093005, arXiv:1612.07377.
[43] S. Goswami, T. Ota, Phys. Rev. D 78 (2008) 033012, arXiv:0802.1434.
[44] S. Antusch, M. Blennow, E. Fernandez-Martinez, J. Lopez-Pavon, Phys. Rev. D 80 (2009) 033002, arXiv:0903.3986.
[45] C.P. Burgess, N.S. Dzhalilov, T.I. Rashba, V.B. Semikoz, J.W.F. Valle, Mon. Not. R. Astron. Soc. 348 (2004) 609, arXiv:astro-ph/0304462.
[46] H. Nunokawa, A. Rossi, V.B. Semikoz, J.W.F. Valle, Nucl. Phys. B 472 (1996) 495, arXiv:hep-ph/9602307.
[47] A.B. Balantekin, J.M. Fetter, F.N. Loreti, Phys. Rev. D 54 (1996) 3941, arXiv:astro-ph/9604061.
[48] C. Burgess, N.S. Dzhalilov, M. Maltoni, T.I. Rashba, V.B. Semikoz, M.A. Tortola, J.W.F. Valle, Astrophys. J. 588 (2003) L65, arXiv:hep-ph/0209094.
[49] C.P. Burgess, N.S. Dzhalilov, M. Maltoni, T.I. Rashba, V.B. Semikoz, M.A. Tortola, J.W.F. Valle, J. Cosmol. Astropart. Phys. 0401 (2004) 007, arXiv:hep-ph/0310366.
[50] K. Abe, et al., T2K, Phys. Rev. D 96 (2017) 011102, arXiv:1704.06409.
[51] K. Abe, et al., T2K, Phys. Rev. Lett. 118 (2017) 151801, arXiv:1701.00432.
[52] M. Hartz, T2K Collaboration, T2K neutrino oscillation results with data up to 2017 summer, http://www.t2k.org/docs/talk/282, 2017.
[53] P. Adamson, et al., NOvA, Phys. Rev. Lett. 118 (2017) 151802, arXiv:1701.05891.
[54] P. Adamson, et al., NOvA, Phys. Rev. Lett. 118 (2017) 231801, arXiv:1703.03328.
[55] A. Himmel, NOvA, New neutrino oscillation results from NOVA, https://indico.cern.ch/event/696410/, 2018.
[56] F.P. An, et al., Daya Bay, Phys. Rev. D 95 (2017) 072006, arXiv:1610.04802.
[57] S.-H. Seo, RENO, in: 15th International Conference on Topics in Astroparticle and Underground Physics (TAUP 2017), Sudbury, Ontario, Canada, 24–28 July 2017, 2017, pp. 24–28, arXiv:1710.08204, http://inspirehep.net/record/1631988/files/arXiv:1710.08204.pdf, 2017.
[58] M.Y. Pac, RENO, arXiv:1801.04049, http://inspirehep.net/record/1647948/files/arXiv:1801.04049.pdf, 2018.
[59] M. Ishitsuka, Double Chooz Collaboration, Double Chooz reactor antineutrino experiment, https://indico.in2p3.fr/event/12279/session/3/contribution/173/material/slides/0.pdf, 2016.
[60] M.G. Aartsen, et al., IceCube, Phys. Rev. D 91 (2015) 072004, arXiv:1410.7227.
[61] S. Adrian-Martinez, et al., ANTARES, Phys. Lett. B 714 (2012) 224, arXiv:1206.0645.
[62] K. Abe, et al., Super-Kamiokande, arXiv:1710.09126, 2017.
[63] Y. Nakano, PhD Thesis, University of Tokyo, 2016, http://www-sk.icrr.u-tokyo.ac.jp/sk/_pdf/articles/2016/doc_thesis_naknao.pdf.
[64] F. Capozzi, E. Lisi, A. Marrone, D. Montanino, A. Palazzo, Nucl. Phys. B 908 (2016) 218, arXiv:1601.07777.
[65] J.K. Ahn, et al., RENO, arXiv:1003.1391, 2010.
[66] J.H. Choi, et al., RENO, Phys. Rev. Lett. 116 (2016) 211801, arXiv:1511.05849.
[67] A. Meregaglia, Double Chooz Collaboration, Multi-detector results from the Double Chooz experiment, https://indico.in2p3.fr/event/13763/session/14/contribution/29/material/slides/0.pdf, 2017.
[68] IceCube Oscillations: 3 years muon neutrino disappearance data, https://icecube.wisc.edu/science/data/nu_osc, 2016.
[69] M. Honda, M. Sajjad Athar, T. Kajita, K. Kasahara, S. Midorikawa, Phys. Rev. D 92 (2015) 023004, arXiv:1502.03916.
[70] M. Honda, Atmospheric neutrino flux updates, http://www.icrr.u-tokyo.ac.jp/~mhonda/, 2015.
[71] A.M. Dziewonski, D.L. Anderson, Phys. Earth Planet. Inter. 25 (1981) 297.
[72] M.G. Aartsen, et al., IceCube, Phys. Rev. Lett. 120 (2018) 071801, arXiv:1707.07081.
[73] I. Esteban, M.C. Gonzalez-Garcia, M. Maltoni, I. Martinez-Soler, T. Schwetz, J. High Energy Phys. 01 (2017) 087, arXiv:1611.01514.
[74] T. Schwetz, M. Tortola, J.W.F. Valle, New J. Phys. 13 (2011) 063004, arXiv:1103.0734.
[75] D.V. Forero, M. Tortola, J.W.F. Valle, Phys. Rev. D 86 (2012) 073012, arXiv:1205.4018.
[76] http://www-sk.icrr.u-tokyo.ac.jp/sk/publications/data/sk.atm.data.release.tar.gz.
[77] T. Collaboration, Neutrino beam flux prediction 2016, http://t2k-experiment.org/result_category/flux/, 2015.
[78] P. Huber, M. Lindner, W. Winter, Comput. Phys. Commun. 167 (2005) 195, arXiv:hep-ph/0407333.
[79] P. Huber, J. Kopp, M. Lindner, M. Rolinec, W. Winter, Comput. Phys. Commun. 177 (2007) 432, arXiv:hep-ph/0701187.
[80] P. Huber, M. Lindner, T. Schwetz, W. Winter, J. High Energy Phys. 11 (2009) 044, arXiv:0907.1896.
[81] S. Sachi Chatterjee, P. Pasquini, J.W.F. Valle, Phys. Rev. D 96 (2017) 011303, arXiv:1703.03435.
[82] S.S. Chatterjee, P. Pasquini, J.W.F. Valle, Phys. Lett. B 771 (2017) 524, arXiv:1702.03160.
[83] F. Capozzi, E. Lisi, A. Marrone, A. Palazzo, arXiv:1804.09678, 2018.